A comparison of lithospheric thickness models

Bernhard Steinberger[a,b,*], Thorsten W. Becker[c]

[a] *GFZ German Research Centre for Geosciences, Telegrafenberg, 14473 Potsdam, Germany*
[b] *Centre for Earth Evolution and Dynamics, University of Oslo, PO Box 1028, 0315 Oslo, Norway*
[c] *Jackson School of Geoscience, The University of Texas at Austin, 10100 Burnet Road (R2200), Austin, TX 78758-4445, USA*

Abstract

The outermost layer of the solid Earth consists of relatively rigid plates whose horizontal motions are well described by the rules of plate tectonics. Yet, the thickness of these plates is poorly constrained, with different methods giving widely discrepant results. Here a recently developed procedure to derive lithospheric thickness from seismic tomography with a simple thermal model is discussed. Thickness is calibrated such that the average as a function of seafloor age matches the theoretical curve for half-space cooling. Using several recent tomography models, predicted thickness agrees quite well with what is expected from half-space cooling in many oceanic areas younger than ≈ 110 Myr. Thickness increases less strongly with age for older oceanic lithosphere, and is quite variable on continents, with thick lithosphere up to ≈ 250 km inferred for many cratons. Results are highly correlated for recent shear-wave tomography models. Also, comparison to previous approaches based on tomography shows that results remain mostly similar in pattern, although somewhat more variable in the mean value and amount of variation. Global correlations with and between lithosphere thicknesses inferred from receiver functions or heat flow are much lower. However, results inferred from tomography and elastic thickness are correlated highly, giving additional confidence in these patterns of thickness variations, and implying that tomographically inferred thickness may correlate with depth-integrated strength. Thermal scaling from seismic velocities to temperatures yields radial profiles that agree with half-space cooling over large parts

*Corresponding author; e-mail: bstein@gfz-potsdam.de, phone: +49-331-288-1881

of their depth range, in particular for averaged profiles for given lithosphere thickness ranges. However, strong deviations from half-space cooling profiles are found in thick continental lithosphere above depth $\approx$ 150 km, most likely due to compositional differences.

Keywords: lithosphere, tomography, half-space cooling, craton, elastic thickness

1. Introduction

The theory of plate tectonics gives a good description of the kinematic behavior of the Earth's surface. Plate tectonics is the surface expression of convection in the Earth's mantle, and in the last $\sim$ 50 years since it was first formulated (e.g., McKenzie and Parker, 1967; Morgan, 1968) a great deal of progress has been made in understanding how a set of plates that are approximately rigid but move relative to each other can arise as a consequence of mantle dynamics, and how the tectonic plates interact with the underlying mantle.

Plates can experience drag as they move over the mantle beneath – which is assumed to behave like a viscous fluid over geologic time scales. This is for example the case, if a plate is mainly pulled by a subducted slab. But plates can also be driven by convection currents in the underlying mantle (e.g., Becker and O'Connell, 2001; Conrad and Lithgow-Bertelloni, 2002; Becker, 2006; van Summeren et al., 2012). Both mechanisms of interaction strongly depend on the thickness of the lithospheric plates: Thick lithospheric keels couple the plates more strongly to the underlying mantle, in particular because below the asthenosphere viscosity increases again with depth. Thicker lithosphere may reach to depths where mantle viscosity is already higher again (e.g., Gurnis and Torsvik, 1994; Zhong, 2001; Conrad and Lithgow-Bertelloni, 2006).

Hence knowledge of lithosphere thickness helps the understanding of plate-mantle interactions. Further, distinguishing thermal and compositional lithosphere is important for, e.g., understanding different contributions to topography (isostatic and dynamic). More generally, an understanding of lithosphere

thickness (both thermal and compositional) is important to address many questions in continental geodynamics.

We envision here the lithosphere as the outermost layer of the Earth that moves more or less coherently as tectonic plates, due to its stronger rheology, and higher viscosity in particular. Rheology relevant for lithosphere thickness may be influenced by thermal and compositional effects (e.g., Lee et al., 2005), and may change gradually with depth. The thickness of lithospheric plates is therefore not sharply defined (with any specific definition being somewhat arbitrary) and also rather poorly known. Furthermore strain rate is a possible important contributor to influencing the depth of the lithosphere-asthenosphere boundary (LAB), as rheology may be strain rate dependent. Therefore, there may be a strain rate gradient across the LAB, with important feedbacks between temperature, strain rate and rheology.

This current situation is not caused by a lack of information. There is a wealth of information from which thickness can be indirectly inferred, but some of these thickness estimates turn out to be rather different. In contrast to the lateral extent of plates, which can be directly mapped (for example, based on geodesy), there is no such direct way to determine their vertical extent.

Here, a new method of deriving radial mantle temperature profiles from seismic tomography is introduced. This method is then used to derive lithosphere thickness by assigning the base of the lithosphere to a temperature isosurface. The rationale behind this approach is that temperature is probably the most important factor controlling lithosphere rheology, in particular viscosity, although composition and strain rate also has an effect. And rheology is what determines the long-term behaviour of mantle materials, whether it is rigid enough to move as a coherent plate, or soft enough to be easily sheared. In other contexts, other characteristics may be important, for example whether material has elastic strength. This leads to a different definition of lithosphere thickness, as material may be hot enough such that it has lost its elastic strength, but it may still be rigid enough to not substantially deform on geologic timescales. Here rather the latter is taken as what distinguishes the lithosphere from the

underlying mantle.

Deviations of the determined temperature profiles from those expected for lithospheric cooling further allow to infer compositional variations. Then a systematic comparison with other thickness estimates is performed. First, we briefly recapitulate the different methods with their advantages and shortcomings. If two methods give different results, it does not mean that one has to be wrong; it can also be that different methods see different aspects of the lithosphere (e.g., Burov and Diament, 1995), for which there is no unique definition (e.g., Eaton et al., 2009; Fischer et al., 2010). We shall first strive to constrain the thermal lithosphere, and then comment on possible complexities due to composition.

In the end, the aim in devising a new lithosphere thickness model is obviously not to solve this issue. Rather, by comparing the new model to a variety of other lithosphere thickness estimates, and comparing these other estimates among each other, we would like to say something about which features of thickness models can be regarded as robust, and where the major uncertainties are.

1.1. Seismic Tomography

Seismic tomography aims at determining v_P and v_S velocity distributions, and the latter are typically better constrained than the former for the uppermost mantle because of the predominant sensitivity of surface waves to v_S. Typically, velocities are expressed in terms of anomalies, i.e. deviations from a global, average reference model that depends on depth only. These deviations in turn depend on temperature, pressure (i.e. depth), and composition and can be linked readily to plate tectonics for the upper mantle (e.g., Zhang and Tanimoto, 1991; Ritzwoller et al., 2004; Priestley and McKenzie, 2006; Lekic and Romanowicz, 2011; Burgos et al., 2014).

Compositional variations probably play an important role inside the lithospheric mantle (e.g., Jordan, 1978; Forte and Perry, 2000; Deschamps et al., 2002; Griffin et al., 2009; Cammarano et al., 2011). In particular, continental mid-lithosphere discontinuities (MLDs) (e.g., Selway et al., 2015; Rader et al.,

2015) may represent compositional layering (e.g., Yuan and Romanowicz, 2010). Mid-lithospheric discontinuities may be common in oceanic lithosphere as well (e.g., Beghein et al., 2014; Auer et al., 2015, and references therein). Beneath the lithosphere, seismic velocity anomalies can perhaps serve better as a proxy for temperature anomalies. However, due to partial melting and resulting variations in volatile content and chemical composition, there could still be non-thermal seismic velocity variations in the asthenosphere (e.g., Goes and van der Lee, 2002).

If one knows the dependence of seismic velocity anomalies on temperature anomalies and depth, and the global average for the temperature versus depth profile, one can in principle convert seismic anomalies to temperature. After assigning a given temperature to the base of the lithosphere, it is then straightforward to derive a lithosphere thickness model.

However, there are difficulties with this approach. Firstly, it is not straightforward to derive the reference profile for temperature versus depth. Mainly, the surface value is known, and approximately the value it approaches at depths corresponding to the thickest lithosphere. Secondly, any compositional anomalies inside the lithosphere will also affect the (global average) reference profile of seismic anomalies. Hence, for example, zero seismic velocity anomaly outside the lithosphere will not correspond to zero temperature anomaly and vice versa. Determining this offset and its dependence on depth is not straightforward either, but it probably overall decreases from a maximum value near the surface to zero at greater depth. Apart from this offset the relation of seismic velocity and temperature anomalies can in principle be determined from mineral physics.

Besides the more principal problems already mentioned, there are also more practical issues: Tomographic inversions often need to be regularized such that the amplitude of recovered seismic velocity anomalies may be less than in reality. They are also affected by smearing: For example, if there is a negative seismic anomaly due to a compositional anomaly inside the lithosphere, and a negative anomaly due to high temperature outside, they may appear as one anomaly due to smearing, hence it may not be possible to determine lithosphere thick-

ness properly. S-wave tomography models typically feature strongly positive anomalies to great depth beneath cratons where thick lithosphere is expected (e.g., Gung et al., 2003). Jordan and Paulson (2013) even suggest a thick tectosphere extending below 350 km depth after applying a smearing correction.

Another, smearing-related problem may occur near subduction zones, if there is a slab underlying the lithosphere but separated by a thin layer of asthenosphere which is not seen by tomography. In this case, lithosphere thickness may be over-estimated. Here, it is attempted to remove slab-related structures approximately by setting tomographic anomalies to zero near the slab contours of the RUM model (Gudmundsson and Sambridge, 1998), and smoothing sharp edges that are introduced by this procedure. This is a conservative estimate of the extent of subducted slabs possibly masking as thick overriding lithosphere, since RUM is based on major, seismically active regions only.

Additional factors that affect the different tomography models are the frequency content of the information used, the varying vertical resolution arising from different parametrizations, and the geographic resolution associated with available path coverage.

Steinberger (2016) implemented an approach of determining lithosphere thickness, and here, for the first time, the procedure and results will be discussed in detail. Essentially, the principal uncertainties are treated by leaving two free parameters that describe the maximum offset (due to compositional anomalies inside the lithosphere) and the length scale over which temperature approaches the adiabat and composition of sublithospheric mantle, and constrain these parameters by matching lithosphere thicknesses determined in the oceans with thicknesses inferred from seafloor ages. This match works quite well for some of the newer tomography models, as will be illustrated in the methods section.

The robustness of the new method will be shown by determining and comparing lithosphere thickness for several recent tomography models, by comparing with results where the lithosphere thickness is simply inferred from an isosurface of tomography, and by comparing with other recent tomography-based lithosphere thickness models (Figure 1), and show that they are all highly cor-

related, despite different procedures. Conrad and Lithgow-Bertelloni (2006) (Figure 1c), for example, use a constant seismic velocity anomaly for depth on continents, and infer thickness from seafloor age in the oceans. Bird et al. (2008) (Figure 1e) use the integrated anomaly over the top 400 km as a proxy for lithosphere thickness on the continents, and again age-dependent thickness in the oceans.

Priestley and McKenzie (2013) (Figure 1d) use a procedure similar to ours, but also constraints from mantle nodules in kimberlites on continents. The LITHO1.0 model of Pasyanos et al. (2014) (Figure 1f) is created by constructing an appropriate starting model and perturbing it to fit high-resolution surface wave dispersion maps (Love and Rayleigh, group and phase). Lithospheric thickness is then defined as the thickness of the high-velocity mantle layer underlying the crust and overlying a lower velocity layer (asthenosphere) that is required to fit the surface wave data. Studies based solely on fundamental mode surface waves start losing resolution around 250 km depth, so they are not optimally suited for determining the thickness of the lithosphere, as they tend to smear images in the vertical direction. This issue is addressed by models such as SAVANI (Auer et al., 2014) using both surface and body waves, and not just fundamental mode data, but also overtones. SL2013 (Schaeffer and Lebedev, 2013) also effectively uses overtones, giving improved vertical resolution.

We note that there are a number of other thermal (and sometimes also compositional) models inferred from seismic models or data in the literature which allow to estimate the thickness of the thermal lithosphere (e.g., Deschamps et al., 2002; Shapiro and Ritzwoller, 2004; Cammarano et al., 2011; Khan et al., 2011), but the aim here is to focus only on a few observational techniques (e.g. tomography vs. impedance-sensing receiver functions) and constraints (e.g. heat flow), and not consider joint modeling approaches for clarity.

1.2. Receiver functions

Figure 1a shows thickness from receiver functions, l_{RF}, from Rychert et al. (2010). Here the "cap version" is shown, where values are adopted from the

nearest data point up to five arc-degrees distance, but different interpolation would yield similar results. The receiver function (RF) method is based on the conversion from P- to S-waves or the other way round, and therefore images rather sharp velocity contrasts. Hence what is interpreted as the base of the lithosphere from RF is not necessarily the same thing physically as what other methods such as tomography would imply (see, e.g., Eaton et al., 2009; Fischer et al., 2010, for reviews). Interpretation of receiver function results in terms of the bottom of the lithosphere is complicated by possibly widespread mid-lithospheric discontinuities (e.g. Romanowicz, 2009; Selway et al., 2015).

1.3. Heat flow

Artemieva (2006) computed lithosphere thickness on continents from geotherms constrained by reliable data on borehole heat flow measurements (l_T in Figure 1b). For comparison, also an inference from a global heat flow compilation (Davies, 2013) is shown in Figure 1j. We here use the inverse of heat flow q as a simple proxy, assuming that $1/q$ is proportional to lithosphere thickness (as, e.g., for half-space cooling), for the sake of argument. The latter has not been corrected for radiogenic heat in the crust, and we mainly show this simple model for comparison with the Artemieva (2006) model, which tries to account for crustal heat production, and for comparison with other models in the oceans, where the Artemieva (2006) model is not defined. In the following we will, among these two models, mainly focus on Artemieva (2006).

1.4. Elastic thickness

Audet and Bürgmann (2011) calculated estimates of the lithosphere's effective elastic thickness over the continents from a comparison of the spectral coherence between topography and gravity anomalies and the flexural response of an equivalent elastic plate to loading (T_E in Figure 1g). The thickness over which the plate reacts elastically is expected to be less that the thickness over which temperature approaches the adiabat (i.e. thermal thickness) or holds equivalent

viscous "strength" (e.g., Burov and Diament, 1995; Watts, 2001). The estimation of elastic thickness depends on fitting in the wavenumber domain and the broad span of wavelengths needed is harder to achieve near continental margins compared to interiors, for example.

In addition to these methods, changes in anisotropy can also give information on lithosphere thickness (e.g., Gung et al., 2003; Debayle and Ricard, 2013; Burgos et al., 2014; Becker et al., 2014; Auer et al., 2015). However, interpretation is complicated and no global lithosphere thickness maps based on anisotropic structure have been published in recent years, although earlier studies (Babuška et al., 1998; Plomerová et al., 2002) and oceanic-only approaches (e.g. Burgos et al., 2014) exist. Hence the comparison will be limited to the four methods based on seismic tomography, heat flow, receiver functions and elastic thickness. Figure 1 shows that these results are already quite different from each other, and we proceed to assess these differences quantitatively.

2. Methods: Determining lithosphere thickness from seismic tomography

The base of the lithosphere is assigned to a given temperature T_L. Its depth is determined from five recent, shear wave tomography models (see Table 1), whereby additional layers may be introduced such that their spacing is at most 25 km. Above the uppermost layer of the original model, values are set equal to that layer; below they are interpolated. We follow these steps:

1. Relative seismic velocity anomalies, δv_S, are assumed to have a thermal component $\delta v_S/v_S|_{th}$ that is proportional to deviations of the actual temperature profile $T(z)$ from the reference profile $T_0(z)$ representing the global average:

$$\delta v_S/v_S|_{th} = -F_{th} \cdot \frac{T(z) - T_0(z)}{T_m - T_s} \tag{1}$$

where T_s is surface temperature and T_m (adiabatic) mantle temperature (Figure 2). F_{th} can be determined from $T_m - T_s$ (e.g., Herzberg et al., 2007) and the sensitivity of seismic velocity to temperature $(dv_S/dT)/v_S$ (e.g.,

Steinberger and Calderwood, 2006). With $T_m - T_s = 1325$ K, which is the difference between the mean value of the range $1280 - 1400$°C (Herzberg et al., 2007) and $T_s = 15$°C, and $(dv_S/dT)/v_S = -1.5 \cdot 10^{-4}$/K, it follows F_{th}=19.9%. However, tomography models could be affected by damping, resulting in lower values of F_{th}. But this would also lead to an under-prediction of model topography amplitude (compared to residual topography), and since it is rather over-predicted (Steinberger, 2016), lower values of F_{th} will not be considered.

2. T_L is chosen such that

$$\frac{T_L - T_s}{T_m - T_s} = \mathrm{erf}(1) = 0.843 \quad \text{or} \quad T_L = T_s + 0.843 \cdot (T_m - T_s) \qquad (2)$$

following Sandwell (2001). This fraction 0.843 is arbitrary, since the thermal lithosphere boundary is probably not sharp if viscosity decreases continuously with temperature. Therefore also some results with fractions 0.9 and 0.78 will be shown to assess the variability arising from the choice of this fraction.

3. T_L can now be converted to a value $\delta v_S/v_S|_{th,L}$ of $\delta v_S/v_S|_{th}$ at the base of the lithosphere, using eq. (1).

$$\delta v_S/v_S|_{th,L} = -F_{th} \cdot \frac{T_L - T_0(z)}{T_m - T_s} =$$

$$= \quad F_{th} \cdot \frac{T_m - T_L}{T_m - T_s} - F_{th} \cdot \frac{T_m - T_0(z)}{T_m - T_s} = 3.1\% - 19.9\% \cdot \frac{T_m - T_0(z)}{T_m - T_s} \qquad (3)$$

where eq. (2) has been used in the last equality.

However, the total relative seismic velocity anomaly at the base of the lithosphere $\delta v_S/v_S|_L$ also has a compositional component, and this is not due to compositional variations at the lithosphere boundary (it shall be assumed that all compositional variations occur inside the lithosphere, away from the boundary), but due to the (global average) reference value being affected by compositional variations inside the lithosphere. So eq. (3) can be modified to

$$\delta v_S/v_S|_L = F_{th} \cdot \frac{T_m - T_L}{T_m - T_s} - F_{th} \cdot \frac{T_m - T_0(z)}{T_m - T_s} + F_C \cdot C_0(z). \qquad (4)$$

Introducing the term $F_C \cdot C_0(z)$ implies that the reference temperature profile does not correspond to the reference seismic profile, rather there is a depth-dependent offset due to compositional variations. The function on the right-hand side shall be called "cutoff function", and lithosphere thickness shall be assigned depending on the value of the relative seismic velocity anomaly $\delta v_S/v_S$ in comparison to the cutoff function. The exact shape of the cutoff function is unknown, but some of its properties can be stated: The term $(T_m - T_0(z))/(T_m - T_s)$ is unity at the surface and approaches zero for large depth, and $C_0(z)$ should have the same properties, if F_C is the surface value of the compositional component. It therefore appears as a reasonable choice to use

$$\delta v_S/v_S|_L = F_{th} \cdot \frac{T_m - T_L}{T_m - T_s} - F_{tot} \cdot \left(1 - \mathrm{erf}\left(\frac{z}{z_0}\right)\right) \tag{5}$$

as cutoff function, as $1 - \mathrm{erf}(z/z_0)$ also has the value 1 for $z = 0$ and approaches zero for large z. This is for example the case if

$$(T_m - T_0(z))/(T_m - T_s) = C_0(z) = 1 - \mathrm{erf}(z/z_0) \tag{6}$$

and $F_{th} - F_c = F_{tot}$, but this is not a necessary condition. Eq. (6) does not imply that temperature follows an error function profile at every point. Rather, it is merely assumed that global mean temperature follows such a profile. z_0 and F_{tot} are two parameter that will be adjusted, as explained below. More generally, this corresponds outside the lithosphere to the equation

$$\delta v_S/v_S = F_{th} \cdot \frac{T_m - T(z)}{T_m - T_s} - F_{tot} \cdot \left(1 - \mathrm{erf}\left(\frac{z}{z_0}\right)\right). \tag{7}$$

Solving this equation for $T(z)$ apparent temperature profiles can be computed. Clear deviations from what appears a reasonable temperature profile can give indications on compositional variations, in particular if at other depth ranges the results agree with expectations.

For simplicity, we have assumed here a linear relation between temperature and velocity anomalies. However, the effect of temperature dependent attenuation on seismic velocities makes this relation non-linear (e.g. Cammarano et al.,

2003; Cammarano and Romanowicz, 2007). To assess the effect of this nonlinearity, we therefore also consider a case where a quadratic term $b \cdot (\mathrm{erf}(z/z_0) - \mathrm{erf}(1))^2$ has been added to the cutoff function eq. 5, corresponding to the next term in the Taylor expansion. We choose a value $b = 21.9\%$, that approximately, by visual comparison, corresponds to Fig. 3b of Cammarano et al. (2003). Also, the cutoff function eq. 5 does not consider depth-dependence of F_{th}. To assess its effect, additionally a case is considered where $F_{th} = 19.9\% \times \left(1 - \frac{4}{15}\frac{z-200\ \mathrm{km}}{200\ \mathrm{km}}\right)$ approximately corresponding to Steinberger and Calderwood (2006), and F_{tot} has been modified accordingly, assuming $F_{tot} = F_{th} - F_c$ and F_c unchanged. Lastly, also cases are considered where 0.843 has been replaced by 0.9 and 0.78, respectively, in eq. 2 to assess the effect of assuming different temperatures for the base of the lithosphere.

Bounds for the maximum value of lithosphere thickness (usually 400 km) and its minimum (usually equal to crustal thickness from CRUST 1.0 (Laske et al., 2013)) are prescribed. Our procedure then yields a unique lithosphere thickness if there is exactly one depth such that $\delta v_S/v_S$ is greater than the cutoff function above, and less below (see Figure 2 B). If there is more than one depth where this is the case, then, for the oceanic regions, the shallowest one is chosen. In this way, no detached slabs or blobs may be included as lithosphere, as long as they are clearly imaged. In continental regions, cases of shallow low-velocity anomalies (presumably due to compositional variations) underlain by high-velocity anomalies, both within the lithosphere, may be common (Lekic and Romanowicz, 2011) and are presumably physically plausible: Therefore, if all options for lithosphere thickness are < 150 km, the largest one is assigned. Only if at least one option is > 150 km, the smallest one of these is chosen. If $\delta v_S/v_S$ is smaller (resp. larger) than the cutoff function at all depths between minimum and maximum, lithosphere thickness is set to the minimum (resp. maximum). Where the uppermost layer of the tomography model is still in the mantle, anomalies are set to taper linearly to zero from the uppermost layer at depth 25 km or less.

For larger values of z_0, the cutoff function, eq. (5) (Figure 2 B), is stretched in the vertical direction and thus shifted towards more negative values for a given depth, and vice versa. This means, more points will be assigned to the lithosphere, resulting in thicker lithosphere values. For larger values of F_{tot}, the cutoff function is also shifted to the left, but more so for shallower depths. This additionally results in a flatter thickness versus age curve. For given z_0 and F_{tot} the average thickness for given ocean floor age intervals is computed. z_0 and F_{tot} are varied until visually an optimal agreement with the theoretical thickness vs. age curve for half-space cooling has been found.

$$z_L = 2\sqrt{\kappa t} = 10 \text{ km}\sqrt{\text{age[Ma]}} \tag{8}$$

with $\kappa = 8 \cdot 10^{-7}\,\mathrm{m^2 s^{-1}}$ for ages less than approximately 100 Ma. Best-fit values for F_{tot} and z_0 vary between 6.2% and 10%, and 120 and 165 km, respectively (see Table 1). The best fits with the theoretical curve are shown in Figure 3. We regard these good fits as an indication that results are also reasonable on continents. However, we have to caution that this calibration implies that the relation between seismic velocities and temperatures is the same for both continents and oceans. The value for κ was adopted from Sandwell (2001). If a value $10^{-6}\,\mathrm{m^2 s^{-1}}$ was used, as is often done, ca. 10% larger thicknesses would result for the theoretical curve. Thus an optimal match would require somewhat larger values for z_0 and/or F_{tot}, leading to somewhat increased lithosphere thickness predictions also elsewhere.

3. Results

3.1. Results based on tomography

Results for lithospheric thickness for this new procedure for different tomography models are shown in Figure 4. Slab related signals have been approximately removed with the procedure as described. Also, a mean thickness model is computed by averaging results for gypsum, s40rts, savani, semum2, and sl2013. This involves mixing estimates based on Voigt average v_S, and on

Table 1: Summary of model parameters. Model: names for tomography model used – gypsum (Simmons et al., 2010), s40rts (Ritsema et al., 2011), savani (Auer et al., 2014), semum2 (French et al., 2013), sl2013 (Schaeffer and Lebedev, 2013). sl2013_dd uses depth-dependent F_{th} and sl2013_nl a non-linear relation between seismic velocity and temperature anomalies (both described in section 2). sl2013_90 and sl2013_78 use values 0.9 and 0.78, respectively, instead of 0.843 in eq. 2 for the base of the lithosphere. F_{tot} and z_0 are parameters of the cutoff function eq. (5), z_{max} is maximum thickness, and $z_{av} \pm z_{std}$ average and standard deviation. For comparison, respective values for the other tomography-based lithosphere thickness models in Figure 1 are also given. Numbers in brackets for z_{max} (323 and 320) indicate that lithosphere thickness found for these models exceeds these values only in very small regions: For semum2 in eastern Tibet (within $92.5^\circ - 95^\circ$ E and $29^\circ - 30^\circ$ N), and around the Persian Gulf (within $47^\circ - 53.5^\circ$ E and $23.5^\circ - 29^\circ$ N), for Pasyanos in Alaska (within $148.5^\circ - 149^\circ$ W and $64^\circ - 64.5^\circ$ N). Also see Table 2 for breakdown by oceanic and continental tectonic regions.

Model	F_{tot}[%]	z_0[km]	z_{max}[km]	$z_{av} \pm z_{std}$[km]
gypsum	9	130	304	97±55
s40rts	8	140	259	94±50
savani	7	160	273	102±60
semum2	6.6	165	373 (323)	100±64
sl2013	6.2	150	347	96±66
sl2013_dd	6.2	150	400	106±61
sl2013_nl	6.2	150	391	114±57
sl2013_90	6.2	150	400	117±75
sl2013_78	6.2	150	300	76±59
Conrad			270	108±54
Priestley			294	117±36
Bird			254	99±46
Pasyanos			460 (320)	107±66

v_{SV} (for models sl2013 and s40rts), but results were not strongly affected by considering radial anisotropy (also see below).

Results of all models shown agree that lithosphere is generally thinner in the oceans and thicker on continents (see also Table 2). Within the oceans,

all models also agree on the trend of lithosphere thickness increasing with age. However, there are some differences as to what extent this tendency of thickening continues to the very oldest lithosphere in the western Pacific: Here, model semum2 (French et al., 2013) yields somewhat larger thicknesses than the other models. This is also evident in Figure 3, where semum2 approximately follows the half-space cooling trend including the very oldest ages, in contrast to the other models.

On the continents, all models agree on greater thickness than elsewhere, up to $\approx$ 250–300 km, for most cratons (outlines e.g. from Bleeker, 2003; Gubanov and Mooney, 2009) including Laurentia, Baltica, Siberia, Amazonia, West Africa, Congo, Kalahari and Australia. Thinner lithosphere (thickness 100 km or less) is found in many regions near ongoing or recent subduction and/or orogeny, including the western United States, western Europe, and eastern Asia. For much of the North China Craton where removal of a cratonic root has been suggested (e.g., Gao et al., 2002), all models indeed predict thicknesses of less than 100 km, in stark contrast to other cratons. However, all models except for gypsum (Simmons et al., 2010) show thickened lithosphere for at least part of the South China Block. Less than 100 km thin lithosphere is also found in northeastern Africa – thinnest around the Afar region, but extending over large regions thousands of km away from it, but also far from any recent orogeny or subduction (see also McKenzie et al., 2015). In general, models show different levels of detail, with whole-mantle tomography models yielding smoother lithosphere structure than upper mantle models. In particular sl2013 (Schaeffer and Lebedev, 2013) yields more fine-scale structure, also showing some features only a few hundred km wide. A limit of resolution is imposed by the choice of expanding tomography models in spherical harmonics, up to a maximum degree and order of 63.

Without removing slabs (results not shown) the contamination of slab structure is quite obvious for some models, particularly sl2013. However, removing slabs also introduces features (e.g. west of the Himalayas) that may not be real. On the other hand, the RUM model does not have slabs in the Himalaya region,

therefore most of our models show thick lithosphere there which may not be real either. In terms of global correlation, though, the removal of slabs hardly matters.

Correlations among thicknesses derived from different, global tomography models are shown in Figure 5 based on spherical harmonic expansions up to degree $\ell = 31$ to focus on the commonly resolved wavelengths. Correlations are generally high, as can also be seen from Figure 4. If a fraction 0.9 of the total temperature contrast between surface and adiabatic mantle is used to define the base of the lithosphere, inferred lithosphere thickness somewhat increases (by $\sim 20\%$ on average; Table 1). Conversely, it somewhat decreases (again by $\sim 20\%$ on average) for a fraction 0.78, but it remains very highly correlated in both cases (correlation 0.98 in Figure 5).

In the case where the non-linearity of the relation between S-wavespeed and temperature is considered in a simplified fashion, predictions for lithosphere thickness become somewhat larger for both very thin lithosphere and very thick lithosphere, but stay similar around the average thickness. In other words, predicted lithosphere thickness variability somewhat increases for thicker lithospheres, and decreases for thinner one. But again, results remain very highly correlated at 0.98. Introducing depth-dependent F_{th} modifies results in a similar way as in the non-linear case, but less strongly so. Accordingly, results are very highly correlated at 0.99 with both the original case and the non-linear case.

For modification cases sl2013_dd, sl2013_nl, sl2013_90 and sl2013_78 values of F_{tot} and z_0 have not been adjusted to optimize the fit (although that could easily be done), because that would complicate assessing the effects of these modifications.

Our procedure relates seismic velocity anomalies (deviations from the mean) to temperature anomalies and accordingly, the degree-zero term (radially symmetric deviation from reference model) in the tomography models has been removed. We also tested how results are affected, if the degree-zero term is kept, and found that inferred lithosphere thickness changes are ~ 1 km.

Overall, these various modelling assumptions have very little effect on the pattern of lithosphere thickness (correlations are very high) but the thickness values themselves, and their variability (characterized by mean and standard deviation in Table 1) are somewhat more strongly affected.

If simply an isosurface of the tomography models is used to define the base of the lithosphere, results remain highly correlated to those results determined with our procedure, generally ~ 0.85. So the pattern of lithosphere thickness determined from tomography is really rather robust, independent of tomography model or method used. Our method is still somewhat heuristic but has more of a physical base, compared to some of the methods used previously. We think that using our method is facilitated by a better vertical resolution of more recent tomography models, which now even allows us to infer a compositional layering of the lithosphere discussed in section 3.3. Previously, lack of vertical resolution supposedly prevented imaging the base of the lithosphere directly, such that other, more approximate procedures had to be used (e.g., Bird et al., 2008).

The average lithosphere thickness and amount of variation is somewhat more dependent on which model and procedure are used. Therefore the relative variations of lithospheric thickness are likely to be better determined than the absolute values. For semum2 and savani, where separate models for SH, SV and Voigt average velocities exist, using identical values for F_{tot} and z_0, the SV models give very similar thickness to the Voigt average, as expected given that $v^2_{S_{Voigt}} = \frac{1}{3}\left(2v^2_{SV} + v^2_{SH}\right)$ for unity ellipticity. The SH model yields somewhat larger thickness (up to few tens of km, for savani, less for semum2) especially for some of the thicker cratons, as expected for a trade-off with radial anisotropy in the asthenosphere (Gung et al., 2003), but SH based patterns are very similar to those for SV or Voigt velocities.

Also, results are generally similar to previous lithosphere thickness models based on tomography, with much higher correlations than with lithosphere thickness models based on other methods (Figure 6). Priestley and McKenzie (2006) obtain quite similar thickness on continents, but a less clear dependence on seafloor age in the oceans. The models of Conrad and Lithgow-Bertelloni

(2006) and Bird et al. (2008) can only be compared on continents, where they are based on older tomography models, and hence either show even less detail (in the first case), or a less clear correlation with cratons (in the second). The LITHO1.0 model of Pasyanos et al. (2014) (Figure 1f) shows the greatest similarities to our results, and even more detail structure. In the Tibetan / Himalaya region, the LITHO1.0 has lithosphere less than $\approx$ 150 km thick, whereas many other tomography-based models show thicker lithosphere there. If lithosphere thickness is computed with our method based on s20rtsb (Ritsema et al., 2004), it becomes visually even more similar to Conrad and Lithgow-Bertelloni (2006), which is based on that tomography model, as expected. For all these and many other models (e.g., Gung et al., 2003; Lekic and Romanowicz, 2011; Jordan and Paulson, 2013), thick lithosphere appears for many cratons.

Mean and standard deviation values for GTR1 (Jordan, 1981) regionalizations are shown in Table 2), for comparison with earlier work. Results are very consistent between models and as expected mirror ocean floor age. Similar to Pasyanos et al. (2014) and Priestley and McKenzie (2013) but different from Bird et al. (2008) and Conrad and Lithgow-Bertelloni (2006), our models tend to show a relatively large thickness for the old lithosphere in the western Pacific, such that the seafloor age vs. lithosphere thickness curve matches the theoretical curve for half-space cooling reasonably well even beyond 100 Ma (Figure 3) (cf., Maggi et al., 2006; Auer et al., 2015).

3.2. Comparison with results based on other methods

In Figure 6 results for the mean, tomography derived thickness model and sl2013 are compared with models derived in a variety of ways. Mean thickness depends on which area is covered. Therefore l_T, which only covers continents, has greater mean thickness than l_S. l_{RF}, which is also mainly determined on continents, however, has similar mean thickness to l_S, although in those regions, where it is determined, it is usually smaller than l_S. Correlations with the mean tomography model are overall somewhat higher than with sl2013, which has been chosen here among the individual models, because it gave the highest

correlations in Figure 5.

Given the uneven geographic coverage, we compute the linear (Pearson) correlation based on an equal area point sampling of the globe and indicate the fraction of the surface sampled by both models in Figure 6. In general, lower correlations are found for those models not based on tomography. A notable exception is the model for elastic thickness (Audet and Bürgmann, 2011), which is highly correlated to tomography-based models, but with elastic thickness being less than the thickness inferred from tomography by a factor $\approx$ 2. For the Audet and Bürgmann (2011) model, elastic thickness also tends to be comparatively high for most cratonic regions, but not for the North China Craton or the South China block. Elastic thickness is rather small (only about 50 km) in the Himalaya / Tibetan region, whereas tomography-based models often feature thicker lithosphere. In Africa, regions of thin elastic lithosphere are mainly near the coasts and in the Afar / Red Sea area. This contrasts to the rather thin lithosphere over wide areas in northeastern Africa found seismologically. In fact, in some areas in Africa, elastic thickness exceeds the thickness determined based on many tomography models.

In the map of Artemieva (2006) based on heat flow, thick lithosphere exceeding $\approx$ 200 km is restricted to rather small areas within cratons, leading to rather low correlations of only slightly above 0.5 with thickness based on tomography. Also, correlations with the inverse of heat flow from Davies (2013) is rather low, indicating that variations of radiogenic element concentrations within the lithosphere, and other compositional heterogeneities, contribute significantly, as expected.

To better understand these results, regional correlations and ratios are plotted in Figure 7. The regional r values are computed based on moving a cap of 1000 km radius with equal area point sampling across the globe after filtering each input model first by a Gaussian smoothing operation of 6σ width of 500 km. We also compute best-fit, linear correlation slopes, b, for regions where $r > 0.3$ allowing for equal errors in both comparison fields. Any such correlations will be dependent on parameter choices but results can give a rough impression of

regional variations in the match between patterns and the typical amplitude ratios.

Overall, the mean values of regional correlations based on the moving cap approach of Figure 7 compare between models in a relative sense that is consistent with what would be inferred from the global correlations shown in Figure 6. However, the absolute r values themselves are somewhat lower for the regional estimates than for the global correlations, which implies that the correlation between models is generally higher at longer wavelengths.

Correlation between tomography and receiver functions is quite variable spatially (Figure 7), and receiver functions tend to give thinner lithosphere, especially in those regions, such as cratons, where thick lithosphere based on tomography is found. This points to the complexity of the interface structure within old continental lithosphere (e.g. Yuan and Romanowicz, 2010; Lekic and Romanowicz, 2011; Fischer et al., 2010; Selway et al., 2015).

Similarly, correlation between receiver functions and elastic lithosphere is rather variable. In general, thickness based on receiver functions correlates better to elastic thickness in those regions where it also correlates better with tomography-based thickness, and vice versa. For example, correlation is relatively high in the western United States and around the Afar Region, where the lithosphere is presumably thin and therefore less complex.

Also, correlation of elastic, receiver-function based, or tomography-based thickness with heat-flow based thickness is quite variable, but with different patterns. Lastly, as expected from the good overall correlation, the correlation between tomography-based and elastic thickness is comparatively high in most regions. One region with rather low correlation, as well as low ratio (b), between tomography-based and elastic thickness, is in northern Africa. Another region with low correlation, but high ratio is the Himalayas and Tibet. In general, the ratio tends to be lower in continental interiors than along margins; elastic thickness determined for continental margins tends to be lower than in the interiors.

Audet and Bürgmann (2011) pointed out the correlation of their T_e values

with anomalies from seismic tomography, and Figure 8 explores this further. A good correlation of T_e with all tomography models used here is found – not only the lithosphere thicknesses based on them, but also the tomography models themselves, above a depth ≈ 200 km. Correlation tends to be somewhat reduced above ≈ 100 km. It reaches a maximum at a depth ≈ 100–200 km, and drops to much smaller and even negative values at greater depth, indicating again that in most regions, the lithosphere does not reach beyond a depth of ≈ 300 km. Taken at face value, the depth-dependent match of tomographic anomalies with T_e would imply that the strength that is sensed by T_e (Burov and Diament, 1995) resides in the lithosphere, not crust. Correlation of elastic thickness with estimates based on heat flow and receiver functions are much lower, as is also evident from Figure 6.

3.3. Compositional stratification?

As a further indication that our procedure gives reasonable results, the apparent temperature versus depth averaged for given lithosphere thickness intervals is plotted in Figure 9. These curves were constructed by first converting profiles of seismic velocity versus depth on a $0.5° \times 0.5°$ grid to apparent temperature versus depth with eq. (7). These profiles are then averaged for given lithosphere thickness ranges but separately for oceanic or continental lithosphere, according to where the Müller et al. (2008) age grid is defined (Figure 1k). For example, the red curve for panel "220" is the average profile for all "continental" grid points, where a lithosphere thickness between 210 and 230 km has been determined. Individual profiles are weighted according to the area represented (proportional to cosine of latitude). Since this was computed assuming thermal scaling between temperature and seismic velocity anomaly locally, but considering the effect of compositionally different lithosphere on the global average, a deviation from what is expected can give an indication for compositional differences. For all except very thin lithospheres it is found that the profiles in their lower parts agree quite well with the theoretical error function profiles. But in particular continental profiles show strong deviations in the upper part (cf.

Lekic and Romanowicz, 2011).

We did the same analysis also for the Voigt velocity of radially anisotropic models semum2 and savani (Auer et al., 2014), to avoid possible trade-off with anisotropy in both oceanic and continental plates (e.g., Gung et al., 2003). Results remain overall similar. For savani, the continental profiles for lithosphere thickness greater than 80 km also show an apparent temperature minimum at similar depths, but not the maximum at even shallower depth. For semum2, profiles for thickness greater than 120 km show again both maximum and minimum at similar depths, with continental and oceanic profiles being very similar to each other for thickness between 180 and 120 km. Also, the overshoot towards inferred normalized temperatures greater than unity is somewhat smaller for the semum2 model. Comparison with the dashed line corresponding to zero seismic anomaly indicates that the deviation from the theoretical error function profiles, at least in the shallower parts of the continental profiles, is most likely not due to damping.

Based on the radial profiles in Figure 9 three different models of a compositional lithosphere are created. For model sl2013_c a thickness 150 km is assigned wherever total thickness exceeds 200 km on continents. Between total thickness 200 and 75 km, compositional thickness decreases linearly from 150 to 75 km. Below thickness 75 km, and in oceanic regions, values for total thickness are adopted. For models sl2013_c2 and sl2013_c3 individual radial profiles instead of the averaged ones are used at each location. In case c3, the maximum of the apparent temperature profile is taken (if there is a local maximum at depth less than the total lithosphere thickness; if there is none total thickness is adopted; if there are several the deepest one is used). In case c2, the average between the local maximum (as in case c3) and the inflection point is used (if there is one at depth less than the total lithosphere thickness and greater than or equal to the maximum; otherwise the total thickness instead of the inflection point is used). Because in many locations, individual radial profiles are similar to the averaged profiles in Figure 9, the different procedures of defining a compositional lithosphere give rather similar and highly correlated results (see also Figure 5).

Based on these compositionally modified models, generally somewhat lower correlations than for the unmodified models (Figure 6) are found. In particular correlations with receiver functions are not improved, but lithosphere thickness values become more similar to the generally smaller thickness determined from receiver functions.

4. Discussion

In the oceanic regions, lithosphere thickness determined with a recently developed procedure versus age matches quite well what is expected from half-space cooling, especially for ages less than about 110 Myr. If the conversion from seismic velocities to temperatures, which is calibrated for the oceans, also holds for the continents, meaningful lithosphere thickness estimates can be derived there. The fact that at least the lower parts of the inferred apparent temperature-versus-depth profiles, averaged for certain lithosphere thicknesses, mostly agrees quite well with theoretical half-space cooling makes this assumption at least plausible.

Deviations of apparent temperature from error function profiles in the upper 100 to 150 km for lithosphere thickness larger than about 100 km in continental regions could be indicative of compositional variations, and their depth range. The shape of this deviation makes it unlikely that this is due to damping. The depth above which deviations occur gets gradually deeper for thicker lithosphere. If lithosphere thickness exceeds 200 km, these deviations mainly occur above 150 km. This is similar to the depths where Yuan and Romanowicz (2010) and Lekic and Romanowicz (2011) propose a compositional layering. One may therefore speculate that this likely compositional effect is linked to the mid-lithospheric discontinuity. Kennett (2015) finds that in Australia a band of P reflectivity commonly occurs close to the mid-lithosphere discontinuity inferred from S wave receiver functions in the cratonic areas.

Thybo (2006) finds a low-velocity zone below a relatively constant depth of 100 km in most continental parts of the world, both in cratonic areas with high

average velocity and tectonically active areas with low average velocity. It is hard to assess whether this is related to the above-mentioned deviations of the apparent temperature from error function profiles, which also occurs for most continental regions, because Thybo (2006) considers absolute velocities, whereas we are concerned with velocity variations relative to a mean.

Profiles for very thin lithosphere – in particular oceanic ones – often show a temperature maximum, which could be due to higher temperatures in the asthenosphere. If non-linearities in the velocity-temperature relation are considered (Cammarano et al., 2003), this maximum is reduced, but the increase in apparent temperature with decreasing depth in continental lithosphere is not affected by considering non-linearity, hence this appears to be a robust feature showing compositional variation. Also, the upper part of oceanic profiles deviates from the theoretical error function profiles. However, the shape is less characteristic and the deviation could at least partly be due to damping. A similar clustering analysis of radial profiles has been performed by Lekic and Romanowicz (2011) and Jordan and Paulson (2013). However, our analysis differs in that we (1) group according to the lithosphere thickness of our model and (2) we convert the seismic to apparent temperature profiles.

The lithosphere thickness models derived here are similar to other recent tomography-based lithosphere models. The LITHO1.0 model of Pasyanos et al. (2014), shown in their Figure 8, and the model of Priestley and McKenzie (2013) (Figure 1) have thick lithosphere in very similar (cratonic) regions. Also, maximum thickness is rather similar in the LITHO1.0 model or semum2 as analyzed by Lekic and Romanowicz (2011), reaching $\gtrsim$ 250 km for some cratons. Gung et al. (2003) find that maximal thickness under cratons is unlikely to exceed 250 km – in agreement with the results obtained here, whereas they conclude, based on anisotropy, that deeper structures are a part of the sublithospheric mantle. In accordance with the radial anisotropy trade-off pointed out by Gung et al. (2003), we obtain somewhat thicker lithosphere with our procedure based on SH models, whereas SV models are very similar to those based on Voigt average (also see Table 2).

Often, thick lithosphere is also inferred for the Tibetan Plateau / Himalaya region (Priestley and McKenzie, 2006), in contrast to thinner lithosphere in other regions of Phanerozoic orogeny. It does not become clear from our work how thick Tibetan lithosphere really is. The traditional view is that this is a region of continental collision, which would explain lithosphere thickening. However, even continental lithosphere may get partially subducted or detach (e.g. Ducea, 2016). In this case, it could be that the lithosphere is in fact not thickened, but due to lack of vertical resolution, the tomography models do not distinguish between the Eurasian lithosphere on top and the subducted Indian lithosphere beneath, and image both as one thick layer (cf. Li et al., 2008). In other regions of subduction, slab signatures have been excluded, but the RUM model of Gudmundsson and Sambridge (1998) which is used for this purpose, does not feature slabs in the Himalaya region, following the traditional view, and we chose not to make any ad hoc adjustments. The fact that elastic lithosphere thickness in the Tibetan / Himalaya region is not higher than in surrounding regions, and that this is the one region where the otherwise good correlation between elastic and tomographic thickness most clearly breaks down (Figure 7) might indicate that indeed the Eurasian lithosphere is not thickened, but underlain by a layer of Indian lithosphere.

Thin lithosphere, similar to orogenic regions, is also found over a rather wide area in northeastern Africa. McKenzie et al. (2015) pointed out that, when reconstructing Pangea, cratons are assembled to one continuous arc of thick lithosphere, surrounding a region of thinner lithosphere that includes northeastern Africa, Arabia and western Europe. Plate reconstructions (Steinberger and Torsvik, 2008; Torsvik et al., 2014) show that northeastern Africa has been overlying the area or margins of the present-day African Large Low Shear Velocity Province in the lowermost mantle for $\sim$ the past 320 Myrs. If this has been a region of upwelling of hot material, this may be a reason for thinner lithosphere. Also presently, material from the Afar plume may be spreading beneath large areas in northeastern Africa and thereby maintaining rather thin lithosphere (e.g. Ebinger and Sleep, 1998; Faccenna et al., 2013).

Lithosphere thickness derived from heat flow measurements (Artemieva, 2006) and receiver functions (Li et al., 2007; Rychert et al., 2010) shows quite a different pattern, with often considerably smaller values. What is inferred to be the lithosphere-asthenosphere boundary (LAB) from receiver functions is interpreted to be considerably sharper than would be expected from only thermal effects, and other explanations have been proposed to explain the sharp LAB (Karato and Jung, 1998; Kawakatsu et al., 2009; Hirschmann, 2010; Karato, 2012; Schmerr, 2012). The issue gets further complicated by the frequent presence of a MLD: What is interpreted as the LAB by receiver function studies may be an MLD. It has been suggested that the lithosphere is chemically distinct mainly above the MLD, whereas the region below is a thermal boundary layer (Yuan and Romanowicz, 2010; Lekic and Romanowicz, 2011).

Our thermal lithosphere models based on tomography are well correlated with the elastic thickness estimates of Audet and Bürgmann (2011). This probably indicates that the elastic thickness and by inference, mechanical strength, is also related to the temperature profile. Elastic thicknesses are typically a factor of about two less than the thickness derived here. This could mean that the lithosphere, on long timescales, behaves elastically only for temperatures up to about half the difference between surface and asthenosphere.

Our lithosphere thickness estimates are meant to represent a temperature isosurface and thus define the depth extent where the mantle is rheologically strong and thus moves coherently as tectonic plates. In a geodynamic context, we regard this as the most appropriate definition, because in this way, lithosphere thickness for example determines how well plates couple with the underlying mantle, and to what extent mantle convection can exert a driving or dragging force. Since temperature increases gradually, strength probably also decreases gradually and lithosphere thickness therefore probably cannot be sharply defined, and any temperature isosurface chosen to define lithosphere thickness is to a certain degree arbitrary.

5. Summary

We present models of lithosphere thickness based on a number of recent tomography models, and a recently developed procedure. The plausibility of these models is demonstrated, because (1) in oceanic regions, they overall agree with thickness inferred from lithosphere age and (2) the lower part of inferred radial temperature profiles, which were used to construct these models agrees quite well with theoretical profiles for half-space cooling, in particular if profiles are averaged for given lithosphere thickness ranges. However, strong discrepancies occur in the upper part of the profiles, in particular for thick continental lithosphere, probably indicating compositional variations mainly in the upper $\approx$150 km. This substantiates earlier results by Lekic and Romanowicz (2011) based on physics-blind, statistical clustering.

Models based on tomography are highly correlated among each other, as well as with other tomography-based lithosphere thickness models. However, average thickness is more dependent on model and procedure. Typically, our model yields lithosphere thickness of about 250 km for cratons, and less in other continental regions. Correlation with thickness estimates based on heat flow and receiver functions are lower. In the case of receiver functions, this could be due to different features "seen" by different methods: The thermal gradients inferred here from tomography is quite gradual, in particular for thick lithosphere, whereas the receiver function method requires sharper discontinuities. Thickness determined here based on tomography is well-correlated with elastic lithosphere thickness, which is typically about a factor two lower.

Acknowledgements

We thank the authors of all models analyzed for making them available, Barbara Romanowicz, an anonymous reviewer and the editor Philippe Agard for helpful comments, and the Humboldt Foundation for making this collaboration possible.

References

Artemieva, I., 2006. Global $1^\circ \times 1^\circ$ thermal model TC1 for the continental lithosphere: implications for lithosphere secular evolution. Tectonophys. 416, 245–277.

Audet, P., Bürgmann, R., 2011. Dominant role of tectonic inheritance in supercontinent cycles. Nature Geosc. 4, 184–187.

Auer, L., Becker, T.W., Boschi, L., Schmerr, N., 2015. Thermal structure, radial anisotropy, and dynamics of oceanic boundary layers. Geophys. Res. Lett. 42, 9740–9742. doi:10.1002/2015GL066246.

Auer, L., Boschi, L., Becker, T.W., Nissen-Meyer, T., Giardini, D., 2014. Savani: A variable-resolution whole-mantle model of anisotropic shear-velocity variations based on multiple datasets. J. Geophys. Res. 119, 3006–3034. doi:10.1002/2013JB010773.

Babuška, V., Montagner, J.P., Plomerová, J., Girardin, N., 1998. Age-dependent large-scale fabric of the mantle lithosphere as derived from surface-wave velocity anisotropy. Pure Appl. Geophys. 151, 257–280.

Becker, T.W., 2006. On the effect of temperature and strain-rate dependent viscosity on global mantle flow, net rotation, and plate-driving forces. Geophys. J. Int. 167, 943–957.

Becker, T.W., Conrad, C.P., Schaeffer, A.J., Lebedev, S., 2014. Origin of azimuthal seismic anisotropy in oceanic plates and mantle. Earth Planet. Sci. Lett. 401, 236–250.

Becker, T.W., O'Connell, R.J., 2001. Predicting plate velocities with geodynamic models. Geochem., Geophys., Geosys. 2. doi:10.1029/2001GC000171.

Beghein, C., Yuan, K., Schmerr, N., Xing, Z., 2014. Changes in seismic anisotropy shed light on the nature of the Gutenberg discontinuity. Science doi:10.1126/science.1246724.

784 Bird, P., Liu, Z., Rucker, W.K., 2008. Stresses that drive the plates from below:
785 Definitions, computational path, model optimization, and error analysis. J.
786 Geophys. Res. 113. doi:10.1029/2007JB005460.

787 Bleeker, W., 2003. The late Archean record: a puzzle in ca. 35 pieces. Lithos
788 71, 99–134.

789 Burgos, G., Montagner, J.P., Beucler, E., Capdeville, Y., Mocquet, A., Drilleau,
790 M., 2014. Oceanic lithosphere/asthenosphere boundary from surface wave
791 dispersion data. J. Geophys. Res. 119, 1079–1093. doi:10.1002/2013JB010528.

792 Burov, E.B., Diament, M., 1995. The effective elastic thickness (T_e) of continen-
793 tal lithosphere: What does it really mean? J. Geophys. Res. 100, 3905–3927.

794 Cammarano, F., Goes, S., Vacher, P., Giardini, D., 2003. Inferring upper-mantle
795 temperatures from seismic velocities. Phys. Earth Planet. Inter. 138, 197–222.

796 Cammarano, F., Romanowicz, B., 2007. Insights into the nature of the transition
797 zone from physically constrained inversion of long-period seismic data. P.
798 Natl. Acad. Sci. USA 104, 9139–9244.

799 Cammarano, F., Tackley, P., Boschi, L., 2011. Seismic, petrological and geo-
800 dynamical constraints on thermal and compositional structure of the upper
801 mantle: global thermo-chemical models. Geophys. J. Int. 187, 1301–1318.

802 Conrad, C.P., Lithgow-Bertelloni, C., 2002. How mantle slabs drive plate tec-
803 tonics. Science 298, 207–209.

804 Conrad, C.P., Lithgow-Bertelloni, C., 2006. Influence of continental roots
805 and asthenosphere on plate-mantle coupling. Geophys. Res. Lett. 33.
806 doi:10.1029/2005GL02562.

807 Davies, J.H., 2013. Global map of solid Earth surface heat flow. Geochem.,
808 Geophys., Geosys. 14, 4608–4622. doi:10.1002/ggge.20271.

809 Debayle, E., Ricard, Y., 2013. Seismic observations of large-scale deformation
810 at the bottom of fast-moving plates. Earth Planet. Sci. Lett. 376, 165–177.

811 Deschamps, F., Trampert, J., Snieder, R., 2002. Anomalies of temperature and
812 iron in the uppermost mantle inferred from gravity data and tomographic
813 models. Phys. Earth Planet. Inter. 129, 245–264.

814 Ducea, M.N., 2016. Understanding continental subduction: A work in progress.
815 Geology 44, 239–240.

816 Eaton, D., Darbyshire, F., Evans, R. L. Grütter, H., Jones, A.G., Yuan, X.,
817 2009. The elusive lithosphere-asthenosphere boundary (LAB) beneath cra-
818 tons. Lithos 109, 1–22.

819 Ebinger, C.J., Sleep, N.H., 1998. Cenozoic magmatism throughout east Africa
820 resulting from impact of a single plume. Nature 395, 788–791.

821 Faccenna, C., Becker, T.W., Jolivet, L., Keskin, M., 2013. Mantle convection in
822 the Middle East: Reconciling Afar upwelling, Arabia indentation and Aegean
823 trench rollback. Earth Planet. Sci. Lett. 375, 254–269.

824 Fischer, K.M., Ford, H. A. Abt, D.L., Rychert, C.A., 2010. The lithosphere-
825 asthenosphere boundary. Ann. Rev. Earth Planet. Sci. 38, 551–575.

826 Forte, A.M., Perry, H.K.C., 2000. Geodynamic evidence for a chemically de-
827 pleted continental tectosphere. Science 290, 1940–1944.

828 French, S., Lekić, V., Romanowicz, B., 2013. Waveform tomography reveals
829 channeled flow at the base of the oceanic asthenosphere. Science 342, 227–
830 230.

831 Gao, S., Rudnick, R.L., Carlson, R.W., McDonough, W.F., Liu, Y.S., 2002.
832 Re–Os evidence for replacement of ancient mantle lithosphere beneath the
833 North China craton. Earth Planet. Sci. Lett. 198, 307–322.

834 Goes, S., van der Lee, S., 2002. Thermal structure of the North American
835 uppermost mantle inferred from seismic tomography. J. Geophys. Res. 107.
836 doi:10.1029/2000JB000049.

837 Griffin, W.L., O'Reilly, S.Y., Afonso, J.C., Begg, G.C., 2009. The composi-
838 tion and evolution of lithospheric mantle: a re-evaluation and its tectonic
839 implications. J. Petrol. 50, 1185–1204.

840 Gubanov, A.P., Mooney, W.D., 2009. New global maps of crustal basement age.
841 Eos Trans. AGU 90. Fall Meet. Suppl., Abstract T53B-1583.

842 Gudmundsson, O., Sambridge, M., 1998. A regionalized upper mantle (RUM)
843 seismic model. J. Geophys. Res. 103, 7121–7136.

844 Gung, Y., Panning, M., Romanowicz, B., 2003. Global anisotropy and the
845 thickness of continents. Nature 422, 707–711.

846 Gurnis, M., Torsvik, T., 1994. Rapid drift of large continents during the Late
847 Precambrian and Paleozoic: Paleomagnetic constraints and dynamics models.
848 Geology 22, 1023–1026.

849 Herzberg, C., Asimow, P.D., Arndt, N., Niu, Y., Lesher, C.M., Fitton, J.G.,
850 Cheadle, M.J., Saunders, A.D., 2007. Temperatures in ambient mantle and
851 plumes: Constraints from basalts, picrites, and komatiites. Geochem., Geo-
852 phys., Geosys. 8. doi:10.1029/2006GC001390.

853 Hirschmann, M.M., 2010. Partial melt in the oceanic low velocity zone. Phys.
854 Earth Planet. Inter. 179, 60–71.

855 Jordan, T.H., 1978. Composition and development of the continental tecto-
856 sphere. Nature 274, 544–548.

857 Jordan, T.H., 1981. Global tectonic regionalization for seismological data anal-
858 ysis. Bull. Seismol. Soc. Am. 71, 1131–1141.

859 Jordan, T.H., Paulson, E.G., 2013. Convergence depths of tectonic regions from
860 an ensemble of global tomographic models. J. Geophys. Res. 118, 4196–4225.
861 doi:10.1002/jgrb.50263.

862 Karato, S.i., 2012. On the origin of the asthenosphere. Earth Planet. Sci. Lett.
863 321–322, 95–103.

Karato, S.i., Jung, H., 1998. Water, partial melting and the origin of seismic low velocity and high attenuation zone in the upper mantle. Earth Planet. Sci. Lett. 157, 193–207.

Kawakatsu, H., Kumar, P., Takei, Y., Shinohara, M., Kanazawa, T., Araki, E., Suyehiro, K., 2009. Seismic evidence for sharp lithosphere-asthenosphere boundaries of oceanic plates. Science 324, 499–502.

Kennett, B.L.N., 2015. Lithosphere-asthenosphere P-wave reflectivity across Australia. Earth Planet. Sci. Lett. 431, 225–235.

Khan, A., Boschi, L., Connolly, J.A.D., 2011. Mapping the Earth's thermochemical and anisotropic structure using global surface wave data. J. Geophys. Res. 116. doi:10.1029/2010JB007828.

Laske, G., Masters., G., Ma, Z., Pasyanos, M., 2013. A 1-degree global model of Earth's crust. Geophys. Res. Abstr. 15. Abstract EGU2013-2658.

Lee, C.T.A., Lenardic, A., Cooper, C.M., Niu, F., Levander, A., 2005. The role of chemical boundary layers in regulating the thickness of continental and oceanic thermal boundary layers. Earth Planet. Sci. Lett. 230, 379–395.

Lekic, V., Romanowicz, B., 2011. Tectonic regionalization without a priori information: A cluster analysis of upper mantle tomography. Earth Planet. Sci. Lett. 308, 151–160.

Li, C., van der Hilst, R.D., Meltzer, A.S., Engdahl, E.R., 2008. Subduction of the Indian lithosphere beneath the Tibetan Plateau and Burma. Earth Planet. Sci. Lett. 274, 157–168.

Li, X., Yuan, X., Kind, R., 2007. The lithosphere-asthenosphere boundary beneath the western United States. Geophys. J. Int. 170, 700–710.

Maggi, A., Debayle, E., Priestley, K., Barruol, G., 2006. Multimode surface waveform tomography of the pacific ocean: a closer look at the lithospheric cooling signature. Geophys. J. Int. 166, 1384–1397.

McKenzie, D., Daly, M.C., Priestley, K., 2015. The lithospheric structure of Pangea. Geology 43, 783–786.

McKenzie, D.P., Parker, R.L., 1967. The North Pacific; an example of tectonics on a sphere. Nature 216, 1276–1280.

Morgan, W.J., 1968. Rises, trenches, great faults, and crustal blocks. J. Geophys. Res. 73, 1959–1982.

Müller, R.D., Sdrolias, M., Gaina, C., Roest, W.R., 2008. Age, spreading rates and spreading asymmetry of the world's ocean crust. Geochem., Geophys., Geosys. 9. doi:10.1029/2007GC001743.

Pasyanos, M.E., Masters, T.G., Laske, G., Ma, Z., 2014. LITHO1.0: An updated crust and lithospheric model of the Earth. J. Geophys. Res. 119, 2153–2173. doi:10.1002/2013JB010626.

Plomerová, J., Kouba, D., Babuška, V., 2002. Mapping the lithosphere-asthenosphere boundary through changes in surface-wave anisotropy. Tectonophys. 58, 175–185.

Priestley, K., McKenzie, D., 2006. The thermal structure of the lithosphere from shear wave velocities. Earth Planet. Sci. Lett. 244, 285–301.

Priestley, K., McKenzie, D., 2013. The relationship between shear wave velocity, temperature, attenuation and viscosity in the shallow part of the mantle. Earth Planet. Sci. Lett. 381, 78–91.

Rader, E., Emry, E., Schmerr, N., Frost, D., Cheng, C., Menard, J., Yu, C.Y., Geist, D., 2015. Characterization and petrological constraints of the midlithospheric discontinuity. Geochem., Geophys., Geosys. 16, 3484–3504. doi:10.1002/2015GC005943.

Ritsema, J., van Heijst, H., Woodhouse, J.H., 2004. Global transition zone tomography. J. Geophys. Res. 109. doi:10.1029/2003JB002610.

Ritsema, J., van Heijst, H.J., 2000. Seismic imaging of structural heterogeneity in Earth's mantle: Evidence for large-scale mantle flow. Sci. Progr. 83, 243–259.

Ritsema, J., van Heijst, H.J., Deuss, A., Woodhouse, J.H., 2011. S40RTS: a degree-40 shear velocity model for the mantle from new Rayleigh wave dispersion, teleseismic traveltimes, and normal-mode splitting function measurements. Geophys. J. Int. 184, 1223–1236.

Ritzwoller, M.H., Shapiro, N.M., Zhong, S., 2004. Cooling history of the Pacific lithosphere. Earth Planet. Sci. Lett. 226, 69–84.

Romanowicz, B.A., 2009. The thickness of tectonic plates. Science 324, 474–476.

Rychert, C.A., Shearer, P.M., Fischer, K.M., 2010. Scattered wave imaging of the lithosphere-asthenosphere boundary. Lithos 120, 173–185.

Sandwell, D., 2001. Cooling of the oceanic lithosphere and ocean floor topography. Available online at `http://topex.ucsd.edu/geodynamics/07cooling.pdf`, accessed 01/2016.

Schaeffer, A., Lebedev, S., 2013. Global shear speed structure of the upper mantle and transition zone. Geophys. J. Int. 194, 417–449.

Schmerr, N., 2012. The Gutenberg discontinuity: Melt at the lithosphere-asthenosphere boundary. Science 335, 1480–1483.

Selway, K., Ford, H., Kelemen, P., 2015. The seismic mid-lithosphere discontinuity. Earth Planet. Sci. Lett. 414, 45–57.

Shapiro, N.M., Ritzwoller, M.H., 2004. Thermodynamic constraints on seismic inversions. Geophys. J. Int. 157, 1175–1188.

Simmons, N.A., Forte, A.M., Boschi, L., Grand, S.P., 2010. GyPSuM: A joint tomographic model of mantle density and seismic wave speeds. J. Geophys. Res. 115. doi:10.1029/2010JB007631.

Steinberger, B., 2016. Topography caused by mantle density variations: observation-based estimates and models derived from tomography and lithosphere thickness. Geophys. J. Int. 205, 604–621.

Steinberger, B., Calderwood, A., 2006. Models of large-scale viscous flow in the Earth's mantle with constraints from mineral physics and surface observations. Geophys. J. Int. 167, 1461–1481.

Steinberger, B., Torsvik, T.H., 2008. Absolute plate motions and true polar wander in the absence of hotspot tracks. Nature 452, 620–623.

van Summeren, J., Conrad, C.P., Lithgow-Bertelloni, C., 2012. The importance of slab pull and a global asthenosphere to plate motions. Geochem., Geophys., Geosys. 13. doi:10.1029/2011GC003873.

Thybo, H., 2006. The heterogeneous upper mantle low velocity zone. Tectonophys. 416, 53–79.

Torsvik, T.H., van der Voo, R., Doubrovine, P.V., Burke, K., Steinberger, B., Ashwal, L.D., Trønnes, R., Webb, S.J., Bull, A.L., 2014. Deep mantle structure as a reference frame for movements in and on the Earth. P. Natl. Acad. Sci. USA 111, 8735–8740. doi:10.1073/pnas.1318135111.

Watts, A.B., 2001. Isostasy and flexure of the lithosphere. Cambridge University Press.

Yuan, H., Romanowicz, B., 2010. Lithospheric layering in the North American continent. Nature 466, 1063–1069.

Zhang, Y.S., Tanimoto, T., 1991. Global Lover wave phase velocity variation and its significance to plate tectonics. Phys. Earth Planet. Inter. 66, 160–202.

Zhong, S., 2001. Role of ocean-continent contrast and continental keels on plate motion, net rotation of lithosphere, and the geoid. J. Geophys. Res. 106, 703–712.

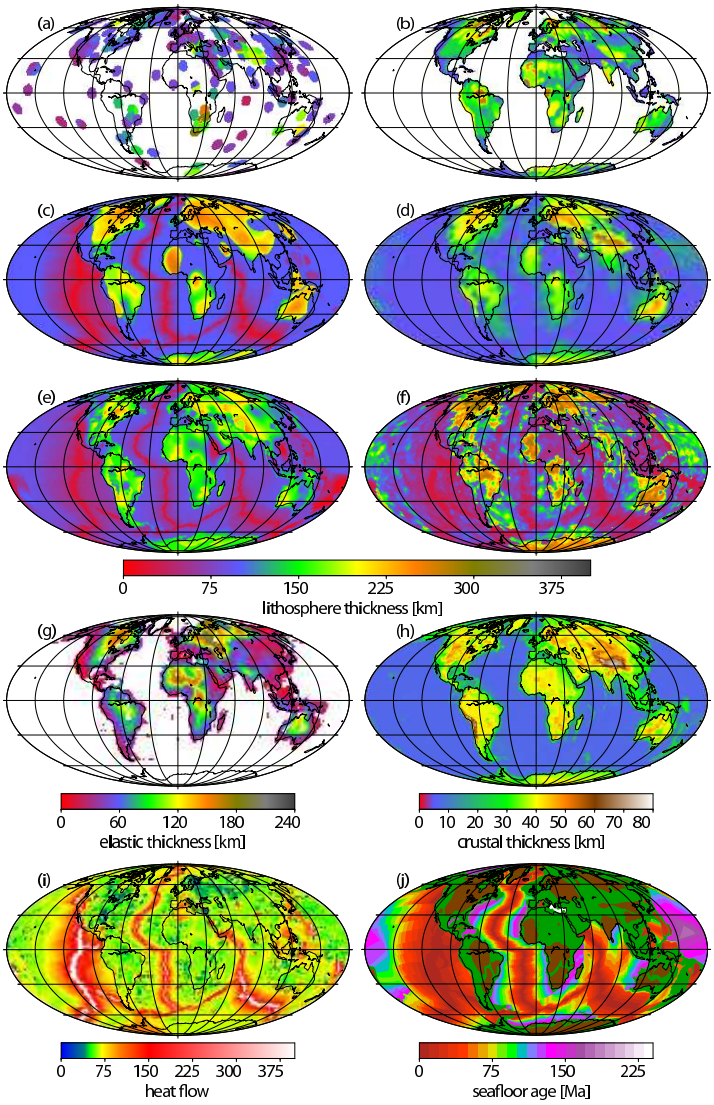

Figure 1: Published lithosphere thickness models and some related quantities. a) l_{RF} inferred from the nearest data point of Rychert et al. (2010) up to five arc-degrees distance; b) l_T Thermal thickness from Artemieva (2006); c) Conrad and Lithgow-Bertelloni (2006), based on tomography model s20rtsb (Ritsema et al., 2004) on continents and an older version of the Müller et al. (2008) age grid; d) Priestley and McKenzie (2013), based on their own surface wave tomography model; e) Bird et al. (2008) based on tomography model s20rts (Ritsema and van Heijst, 2000) on continents and an older version of the Müller et al. (2008) age grid; f) l_{LITHO1} from Pasyanos et al. (2014); g) T_e elastic thickness from Audet and Bürgmann (2011); h) Crustal thickness from CRUST 1.0 (Laske et al., 2013); j) Heat flow (Davies, 2013); k) Seafloor ages (Müller et al., 2008). Cratons from Gubanov and Mooney (2009) in brown, other continents dark green.

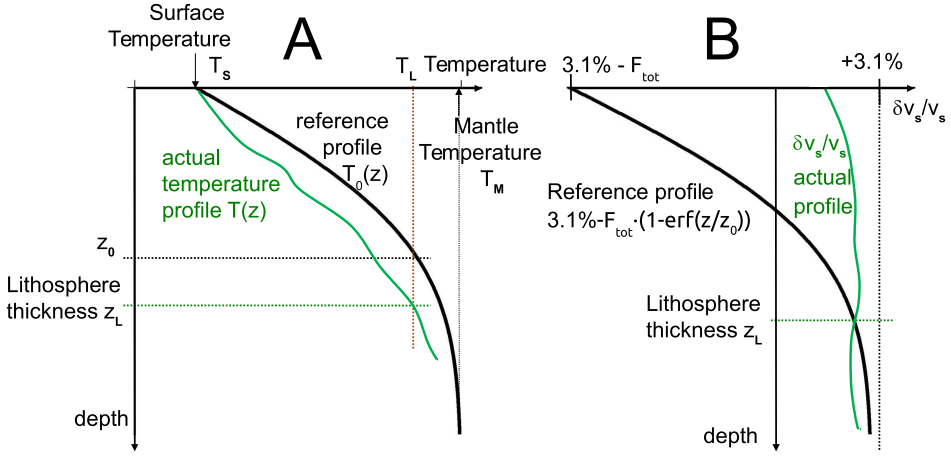

Figure 2: A: Sketch of reference and actual temperature profile, lithosphere thickness z_L and reference thickness z_0. B: Corresponding sketch of seismic velocity anomaly and cutoff function.

Table 2: Lithosphere thickness (average and standard deviation in km) determined for the different GTR1 (Jordan, 1981) tectonic regimes. Tomography models as in Table 1.

model	oceanic	young oc.	intermed. oc.	old oc.	continental	orogenic	Phanerozoic	Precambrian
sl2013	73 ± 37	38 ± 21	75 ± 32	104 ± 33	131 ± 82	95 ± 74	174 ± 72	182 ± 61
gypsum	74 ± 32	38 ± 17	76 ± 25	106 ± 20	134 ± 62	101 ± 45	173 ± 58	179 ± 54
s40rts	74 ± 31	42 ± 18	75 ± 25	107 ± 20	125 ± 57	99 ± 50	155 ± 52	162 ± 40
savani	77 ± 32	48 ± 13	76 ± 25	111 ± 28	140 ± 71	110 ± 67	175 ± 59	187 ± 48
semum2	75 ± 39	35 ± 17	75 ± 30	117 ± 33	140 ± 74	106 ± 64	181 ± 66	188 ± 56
mean	75 ± 31	40 ± 13	75 ± 24	109 ± 22	134 ± 64	102 ± 54	171 ± 57	179 ± 47

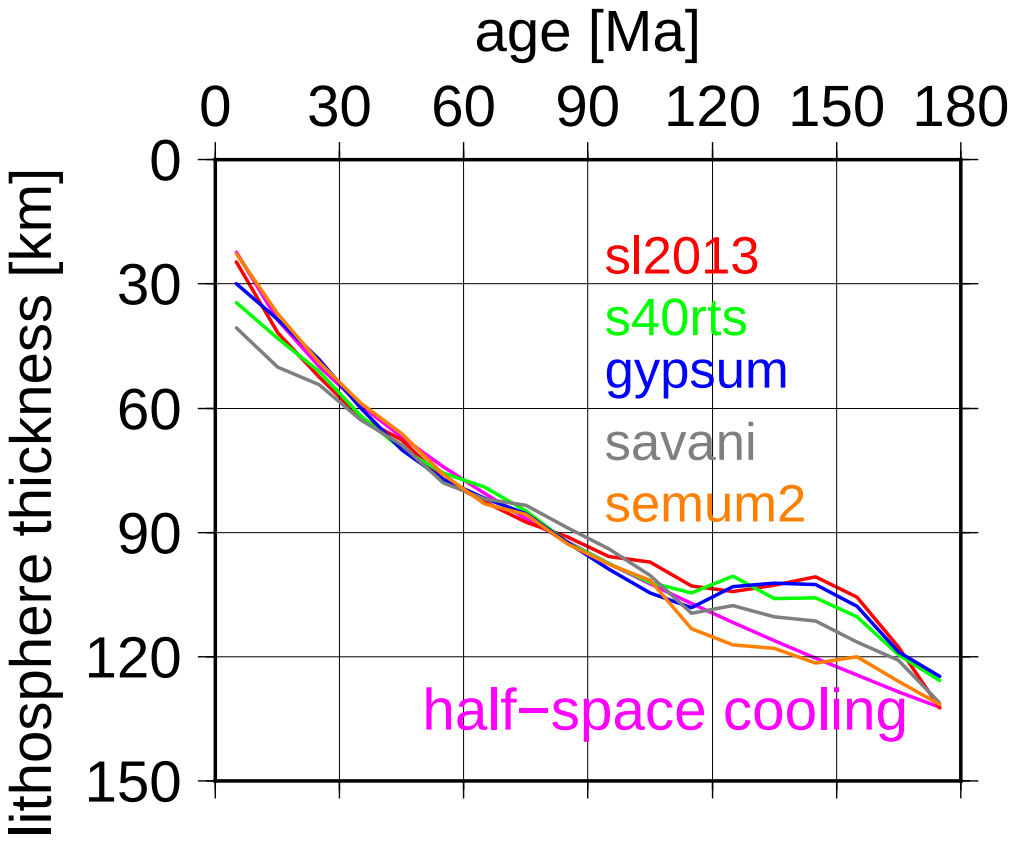

Figure 3: Violet line: Lithosphere thickness $z_L[\mathrm{km}] = 10\sqrt{\mathrm{age[Ma]}}$ obtained from half-space cooling model. Other lines: Average lithosphere thickness for given sea-floor age determined for tomography models as indicated.

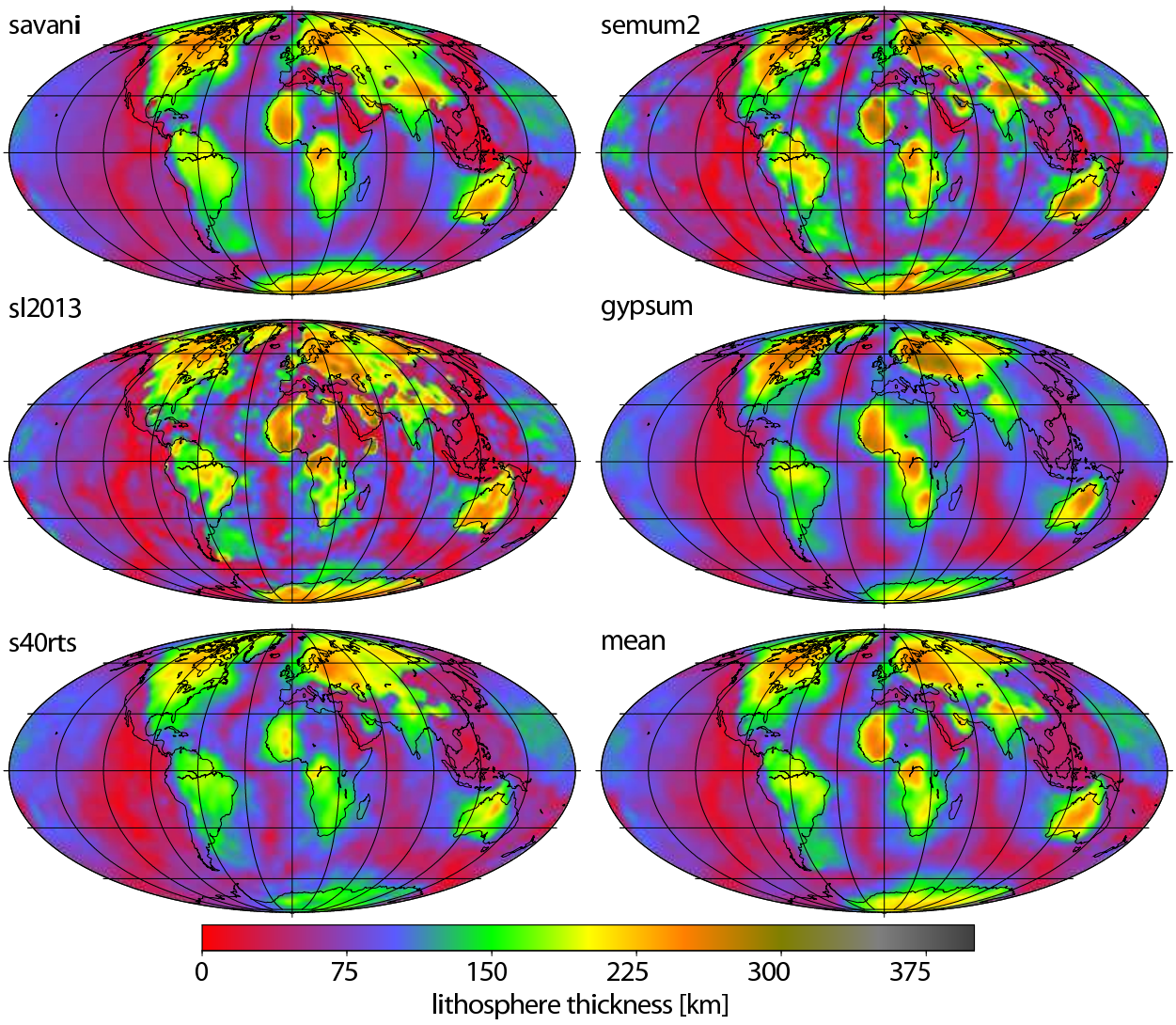

Figure 4: Map views of lithosphere thickness determined with our procedure for different tomography models: gypsum (Simmons et al., 2010), s40rts (Ritsema et al., 2011), savani (Auer et al., 2014), semum2 (French et al., 2013), and sl2013 (Schaeffer and Lebedev, 2013). The mean model is an average of these five models. In all cases, slabs-associated anomalies have been approximately corrected for, as described in the text.

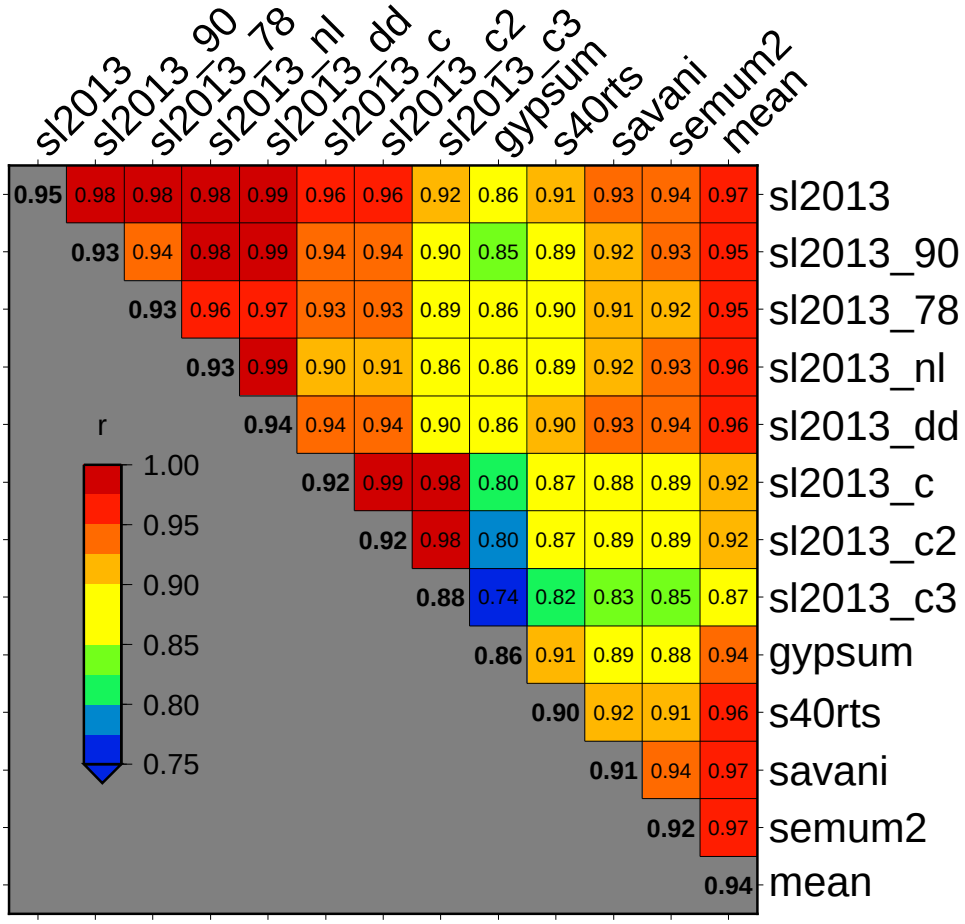

Figure 5: Correlations for lithosphere thickness model determined from tomography (cf. Figure 4) based on spherical harmonic expansions up to degree $\ell = 31$. sl2013_90 and sl2013_78 uses a fraction 0.9 and 0.78, respectively, instead of 0.843 for the base of the lithosphere. sl2013_dd uses a depth-dependent F_{th} and sl2013_nl accounts for non-linear relation between seismic velocity and temperature anomalies (both described in section 2). sl2013_c, sl2013_c2, and sl2013_c3 are three models for a chemically layered lithosphere, as described in the text. Numbers on diagonal give average correlation for each model.

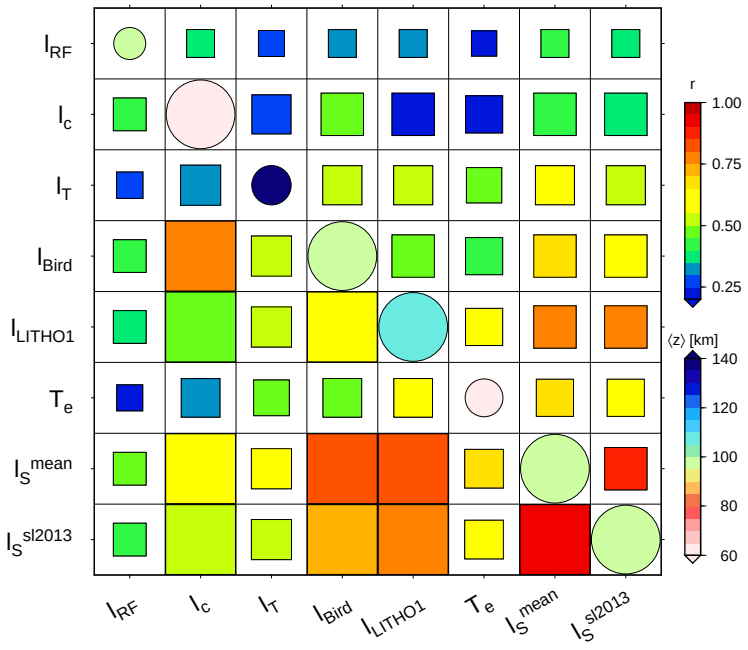

Figure 6: Cross-correlations between thickness models. Lower left of matrix shows global, upper right continent-only correlation, r, respectively, with symbol size scaled with the fraction of the surface covered. Diagonal shows mean thickness values, $\langle z \rangle$. Models: l_{RF}: based on receiver functions (Rychert et al., 2010), l_c: crustal thickness from CRUST 1.0 (Laske et al., 2013), l_T: thermal lithospheric thickness from Artemieva (2006), l_{Bird}: lithospheric thickness from Bird et al. (2008), l_{LITHO1}: lithospheric thickness from Pasyanos et al. (2014), T_e: elastic thickness from Audet and Bürgmann (2011), l_S: tomographically determined thickness (our method), mean model and sl2013.

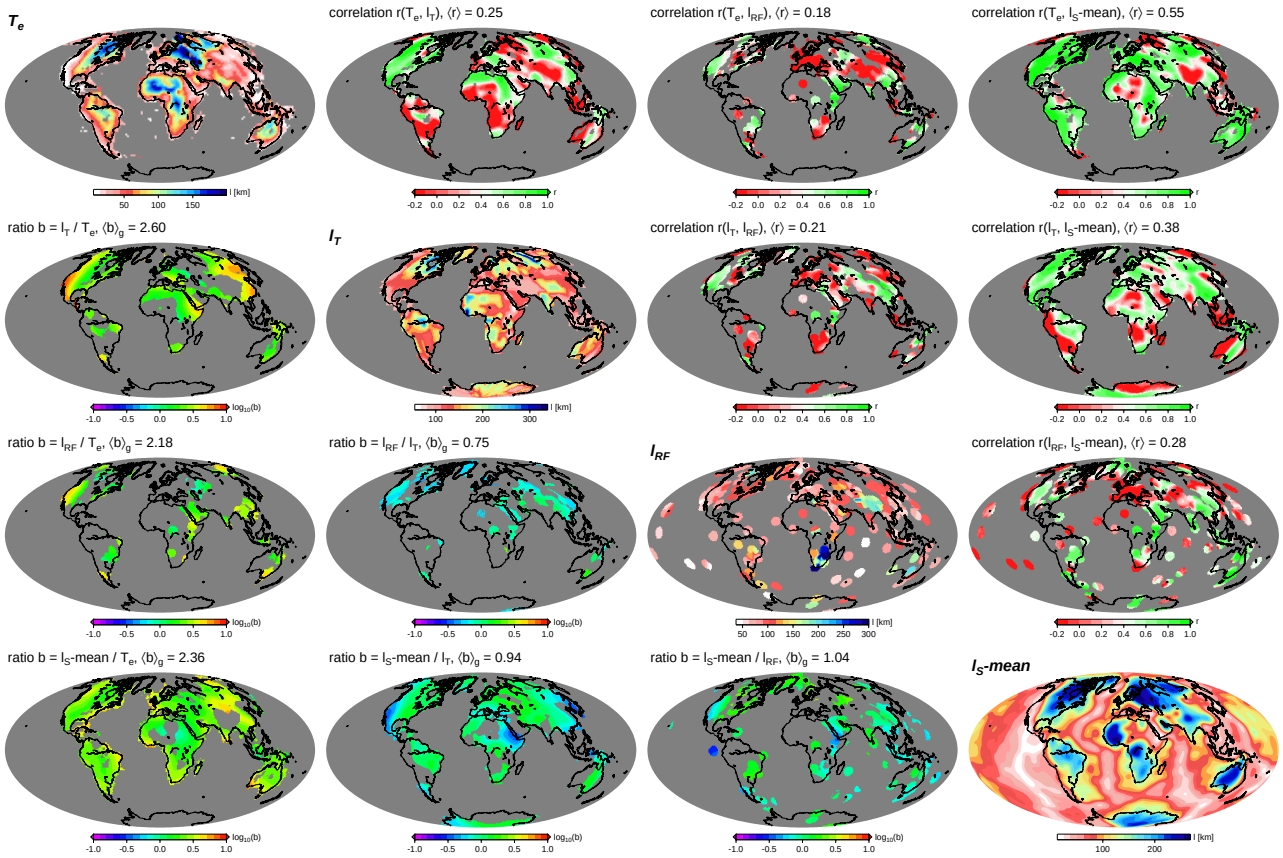

Figure 7: Map views of smoothed lithospheric thickness maps along diagonal (compare Figure 1): Elastic thickness, T_e (Audet and Bürgmann, 2011), thermal lithosphere, l_T (Artemieva, 2006), receiver functions, l_{RF} (Rychert et al., 2010), and the mean, tomographically determined thickness model, l_S. A $6\sigma = 500$ km width, Gaussian smoothing filter was applied. Upper, right part of the plot matrix shows the regional correlations, r, computed from moving a 1000 km radius cap across the domain, and their global mean, $\langle r \rangle$. Lower, left part shows the best-fit linear ratios, b, plotted as $\log_{10}(b)$ for all regions where $b \geq 0.3$, with geometric mean given as $\langle b \rangle_g$.

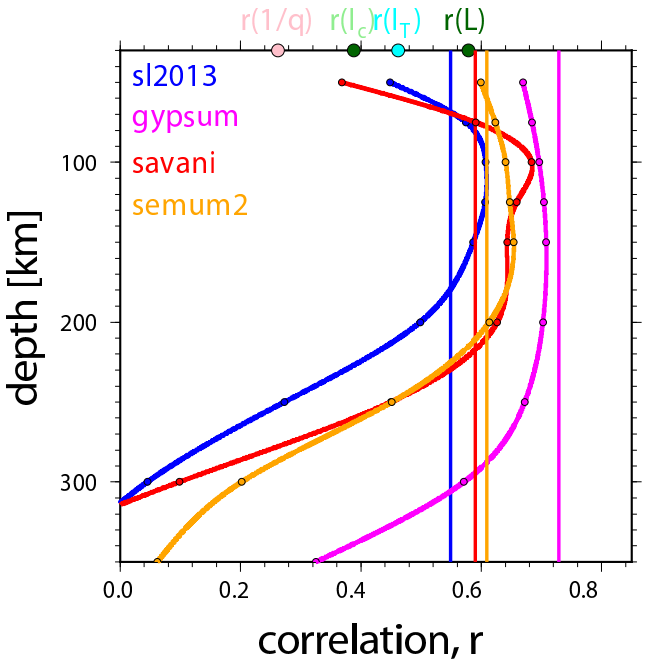

Figure 8: Correlations with elastic thickness, T_e, from Audet and Bürgmann (2011). Depth-dependent curves are correlations with tomography models' velocity anomalies as a function of depth, vertical lines with lithosphere thickness determined from these tomography models. On the top x-axis, $r(1/q)$ denotes the correlation with the inverse of heat flow from Davies (2013), $r(l_c)$ crustal thickness from CRUST 1.0 (Laske et al., 2013), $r(l_T)$ lithosphere thickness from Artemieva (2006) and $r(L)$ lithospheric thickness from Pasyanos et al. (2014). (For other cross-correlations, see Figure 6).

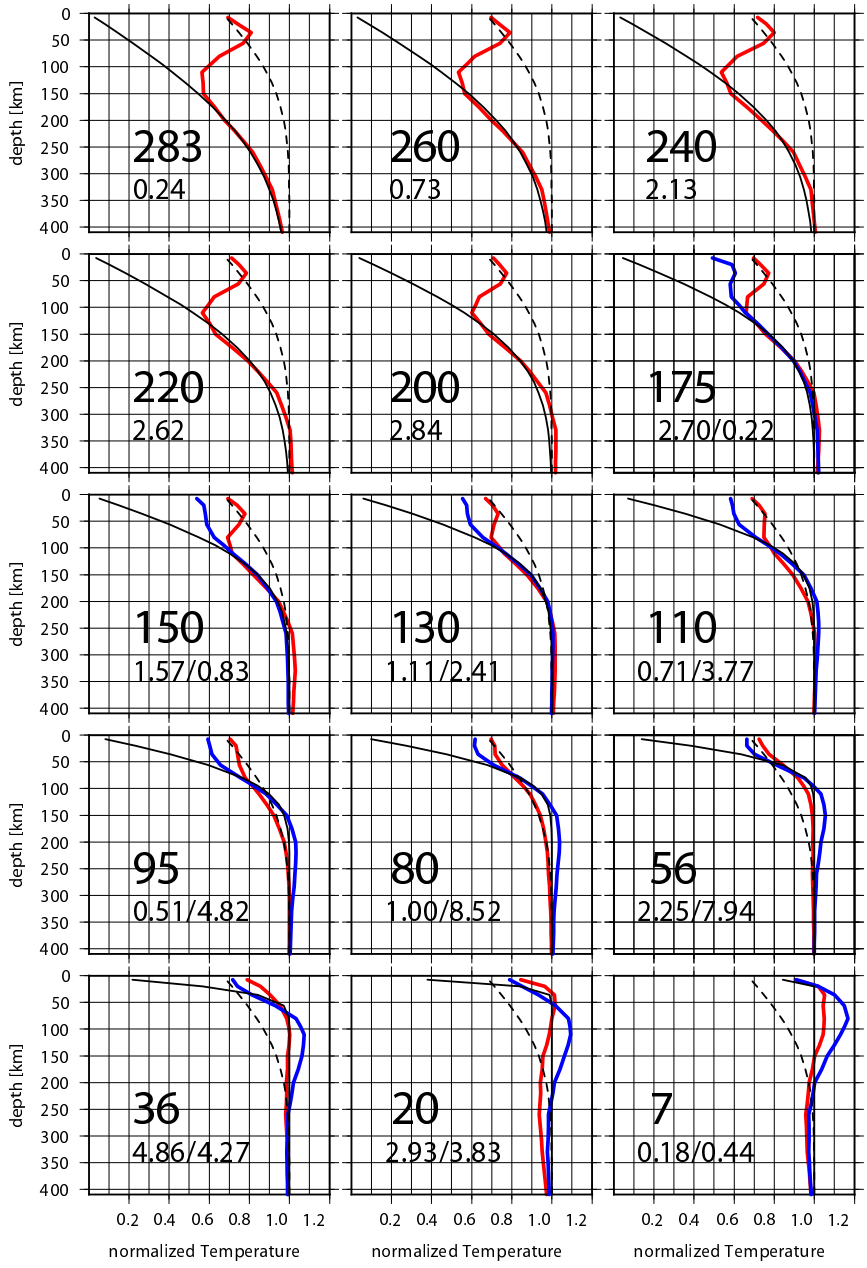

Figure 9: Profiles of averaged and normalized apparent temperature $(\overline{T}(z)-T_s)(T_m-T_s)$, converted from tomography using eq. (7) for given lithosphere thickness intervals, and separately for continents (red) and oceans (blue), for sl2013 (Schaeffer and Lebedev, 2013) tomography. Large numbers indicate values on which thickness intervals are centered. Black lines are error function profiles for this thickness. Black dashed line is the curve that would be inferred for zero anomaly. Small numbers indicate the percentage of total Earth surface area represented by the oceanic/continental curve. Only curves representing more than 0.1% of surface area are plotted.